Length Scale Effect in Frictional Aging of Silica Contacts

Shen Li,[1,*] Shuai Zhang,[1] Zhe Chen,[1] Xi-Qiao Feng,[1,2] and Qunyang Li[1,2,†]
[1]AML, Department of Engineering Mechanics, Tsinghua University, Beijing 100084, China
[2]State Key Laboratory of Tribology, Tsinghua University, Beijing 100084, China

(Received 24 June 2020; revised 4 September 2020; accepted 7 October 2020; published 19 November 2020)

Friction between two solid surfaces often exhibits strong rate and slip-history dependence, which critically determines the dynamic stability of frictional sliding. Empirically, such an evolutional effect has been captured by the rate-and-state friction (RSF) law based on laboratory-scale experiments; but its applicability for generic sliding interfaces under different length scales remains unclear. In this Letter, frictional aging, the key manifestation of the evolutional behavior, of silica-silica contacts is studied via slide-hold-slide tests with apparent contact size spanning across 3 orders of magnitude. The experimental results demonstrate a clear and strong length scale dependency in frictional aging characteristics. Assisted by a multiasperity RSF model, we attribute the length scale effect to roughness-dependent true contact area evolution as well as scale-dependent friction stress due to nonconcurrent slip.

DOI: 10.1103/PhysRevLett.125.215502

Friction of solids, including rock [1,2], rubber [3], metal [4], and other materials [5–7], often exhibits strong sliding velocity and slip-history dependence, which can be fundamentally traced down to the aging of contact interfaces [8–12]. Such evolutional behavior is critical for understanding the sliding instabilities of various frictional systems, ranging from nanoelectromechanical devices to natural faults [7,13–18]. Empirically, friction evolution is described by the rate-and-state friction (RSF) laws [1,2,19,20], where friction coefficient is a function of slip velocity V and phenomenological state variable θ, i.e., $\mu = \mu_0 + a\ln(V/V_0) + b\ln(V_0\theta/D_c)$. The second term, with prefactor a, depicts a direct velocity dependency that is often assumed to stem from thermal activation effect [16]. While the third term, with prefactor b, describes a slip-history dependency through state variable θ that can evolve with slip according to the slip law [2,20], e.g., $d\theta/dt = -(V\theta/D_c)\ln(V\theta/D_c)$, or time according to the slowness law [1], e.g., $d\theta/dt = 1 - (V\theta/D_c)$. Such phenomenological laws are based on the frictional aging phenomenon, a key manifestation of the evolutional behavior, where static friction is found to increase linearly with a logarithm of hold time when a contact interface is held stationary [1].

Although time-dependent variations in true contact area and strength of interfacial bonds have been proposed to account for the friction evolution [21–24], the key RSF parameters still have to be determined by fitting laboratory-scale experiments. For rock friction experiments, mostly with sample size of 1–20 cm, the frictional aging parameter b was found to lie between 0.001 and 0.015 [19,21]. A recent study on frictional behavior of microscale Si devices indicated that the magnitude of frictional aging might be slightly larger (with $b \sim 0.024$) [14]. Although the frictional aging parameter was not explicitly extracted, friction tests using atomic force microscope (AFM) by Li *et al.* [24] suggested that the effect of frictional aging for nanometer-scale contacts could be orders of magnitude stronger than macroscale experiments. So far, RSF experiments were typically conducted at a single length scale [1,19,25], so it is not clear whether the RSF law fitted from that particular scale works for frictional systems of other scales. This question is essential if one wants to extrapolate the laboratory-scale RSF law to various nanometer- or geo-scale phenomena. To address this critical issue, frictional aging behavior was explored via slide-hold-slide (SHS) tests for silica-silica contacts with probe size ranging from nanometer to millimeter scales. To make quantitative comparisons, contacting materials, loading, and data extraction schemes were kept consistent as much as possible. The experimental results showed that the effect of frictional aging decreased in orders of magnitude from nanometer-scale probe to millimeter-scale probe. By normalizing the frictional aging parameter by the steady-state friction coefficient, we found that the strong length scale effect might originate from size-dependent friction shear stress, as qualitatively predicted by a multiasperity RSF model.

The SHS experiments were conducted by sliding silica probes or microspheres on oxidized silicon wafer substrates on an AFM for nanometer- and micrometer-scale tests and on a tribometer for millimeter-scale tests. The nanometer-scale probes were made from commercial silicon AFM probes thermally oxidized in pure oxygen. Silica microspheres attached to tipless AFM cantilevers were used as microscale probes. For millimeter-scale tests, silicon balls with a nominal radius of 1 mm were thermally oxidized with the same protocol and used in the tribometer. Before each test, the surfaces of thermally oxidized silicon wafers were cleaned with Piranha solution for 20 min and

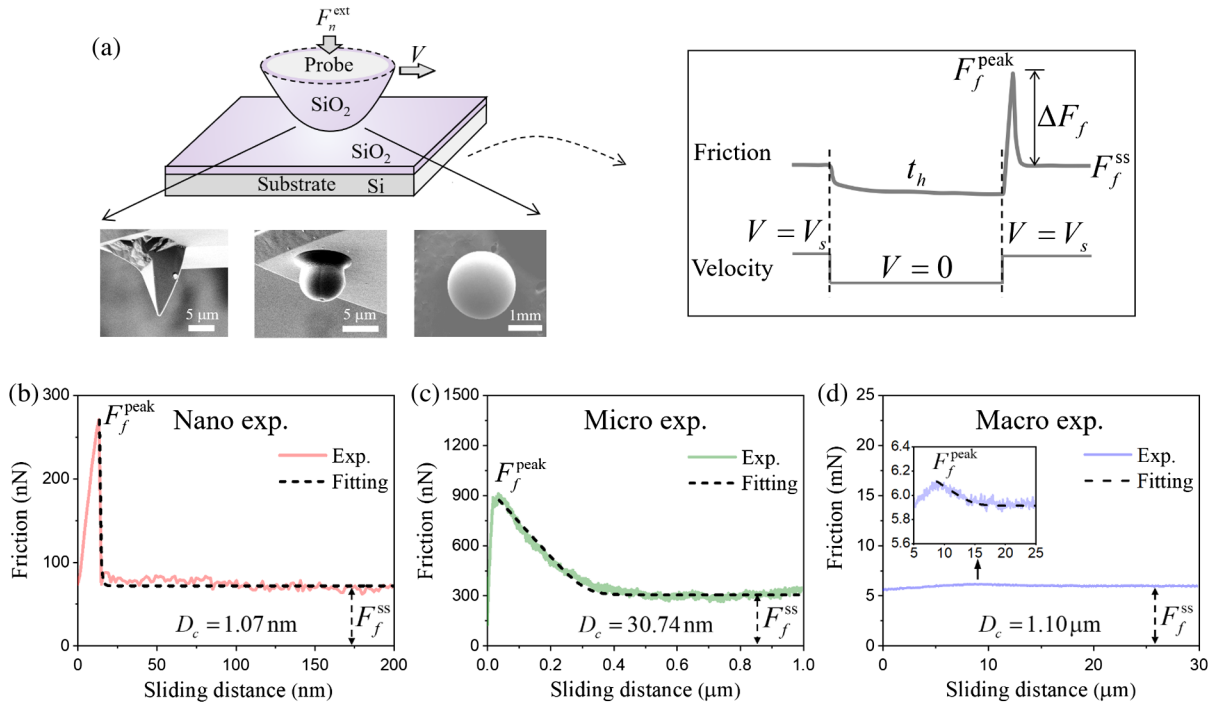

FIG. 1. (a) A schematic showing the experimental setup of SHS tests: Probes at three different size scales, i.e., thermally oxidized AFM tip, silica microsphere, and silica ball (left panel); lateral force and velocity profiles during SHS tests (right panel). Typical friction evolution curves for (b) nanometer-scale, (c) micrometer-scale, and (d) macroscale tests. The friction curve is locally magnified in the inset in (d) for the macroscale test. The fitted parameter D_c and fitted curves (represented by the dashed lines) are shown in (b)–(d). Results in (b)–(d) were obtained in the following conditions: hold time $t_h = 100$ s, sliding velocity $V_s = 3$ μm/s, and RH = 40%. The external applied loads for the nanometer-scale, micrometer-scale, and millimeter-scale experiments were 11.32 nN, 293.66 nN, and 20 mN, respectively, and the resultant apparent contact radii were 6.2 nm, 46.3 nm, and 7.38 μm, respectively (see Supplemental Material, Sec. III [26]).

subsequently rinsed by deionized water and dried under pure nitrogen flow (more details about sample preparation can be found in Supplemental Material, Sec. I [26]).

As schematically illustrated in Fig. 1(a), the SHS test was conducted as follows. Under a fixed external normal load F_n^{ext}, the spherical probe was first slid at a steady velocity V_s, and then the velocity was reduced to zero; after being held stationary for a period of time t_h, the probe was reloaded and slid at the same velocity V_s. Figures 1(b)–1(d) show the typical friction variations for SHS tests under a same period of hold time ($t_h = 100$ s) at three length scales. It is clear that the relative frictional aging behavior, represented by the frictional aging during stationary hold relative to the steady-state friction, $(F_f^{\text{peak}} - F_f^{\text{ss}})/F_f^{\text{ss}}$, differs significantly from 282% and 218% at the nanometer and micrometer scales, respectively, to 3% at the millimeter scale. Meanwhile, the characteristic slip length D_c increases by orders of magnitude when the probe size changes from nanometer scale to millimeter scale (see more details in Supplemental Material, Sec. II [26]).

To quantitatively study the frictional aging characteristics in the classic RSF formulism, the measured friction force needs to be converted to a friction coefficient. As indicated by the typical experimental data shown in Supplemental Material, Sec. IV [26], the steady-state friction vs external normal load data for the experiments at the three length scales all exhibit good linear relationship. However, as the influence of adhesion is non-negligible, to avoid an ill-posed definition of friction coefficient [33–35], we measured adhesion force independently by finding the maximum tensile force needed to pull the probe away from the substrates. Then the measured pull-off forces (7.53 nN, 1.14 μN, and 0.88 mN for the nanometer-scale, micrometer-scale, and millimeter-scale probes, respectively) were added to the external normal load to obtain the effective normal load, i.e., $F_n = F_n^{\text{ext}} + F_n^{\text{ad}}$. Consequently, static peak friction coefficient μ^{peak}, steady-state friction coefficient μ^{ss}, and aging coefficient $\Delta\mu$ can be defined as $\mu^{\text{peak}} = F_f^{\text{peak}}/F_n$, $\mu^{\text{ss}} = F_f^{\text{ss}}/F_n$, and $\Delta\mu = \mu^{\text{peak}} - \mu^{\text{ss}}$, respectively. In this way, the friction coefficients are independent of the normal load within the load range we measured.

Figure 2 shows the variations of aging coefficient $\Delta\mu$ with hold time t_h for SHS experiments at three length scales. To make sure that the influence of wear on friction measurements was minimum, the SHS experiments were carried out by ramping up the hold time from 0.1 to 100 s and then down to 0.1 s. Consistent with previous macroscopic SHS tests for quartz [1,19,21,36], the aging

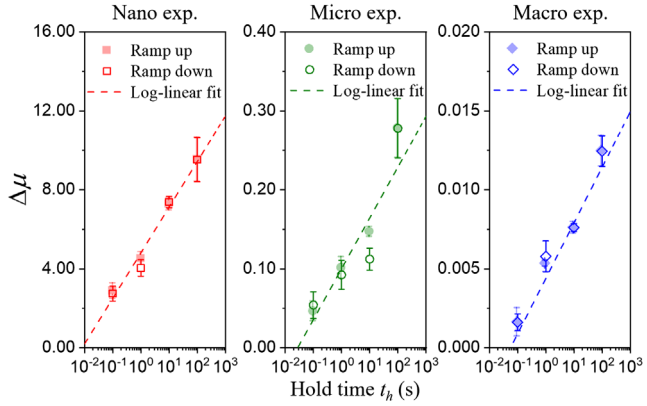

FIG. 2. Variations of frictional aging coefficient with hold time measured in nanometer-, micrometer-, and macroscale experiments. Each data point is an average of five repeated tests. The experimental conditions remain the same as those for Fig. 1.

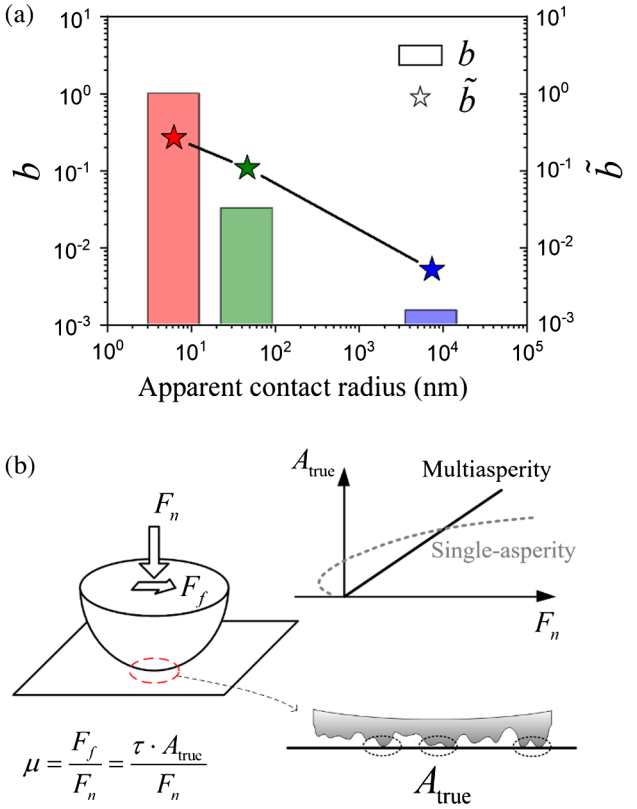

FIG. 3. (a) b and $\tilde{b}$ extracted from the SHS experiments in Fig. 2 at three length scales. (b) A schematic showing that the friction coefficient can depend on friction shear stress and true contact area-load relation, both of which can be scale dependent.

coefficient $\Delta\mu$ varies linearly with the logarithm of hold time for all tests. However, it is obvious that the magnitude of $\Delta\mu$ and the corresponding slope for nanoscale experiments are more than one order of magnitude higher than those for microscale experiments. A similar order-of-magnitude difference also exists between the microscale and the macroscale experimental results. We confirmed that such a strong scale effect was reproducible regardless of humidity (see Supplemental Material, Sec. V [26]).

Based on the SHS data, the evolution parameter of RSF law, b, can be determined by finding the slope of the $\Delta\mu$ vs $\ln t_h$ curve [36]. As shown by the column bars in Fig. 3(a), the extracted values of b for silica-silica contacts vary significantly from 0.9895 for the nanometer-scale tests to 0.0323 for the micrometer-scale tests and finally to 0.0015 for the millimeter-scale tests. This orders-of-magnitude difference clearly demonstrates that the evolution parameter of RSF law is length-scale dependent even for interfaces with identical mating materials.

Previously, Li and co-workers [37] found that higher local pressure would lead to more prominent aging. To check whether the difference in contact pressure can explain the length-scale-dependent behavior observed in our experiments, we compared the contact pressure of these experiments. Based on an adhesive contact mechanics model [27], the average apparent contact pressures for the nanoscale AFM tip, microsphere, and millimeter-scale silica ball are 0.16, 0.21, and 0.12 GPa, respectively (see Supplemental Material, Sec. III [26]). The apparent contact pressures are about the same level. Moreover, if we further consider the roughness of the microsphere and millimeter-scale silica ball, the true contact pressure for microscale and millimeter-scale tests might be even higher. However, in our experiments, the frictional aging is the most significant for the nanometer-scale AFM probes. Therefore, the length scale effect in frictional aging observed in our experiments is unlikely to be caused by the difference in contact pressure.

Recently, it has been shown that the aging effect can be weakened due to premature perturbation if lateral loading induces torque along the contact interface [38]. Among the three experiments in this work, the nanoscale and microscale tests are possibly affected by torque, since the AFM cantilever uses a twist mode to sense friction. However, the torque effect is minimized for millimeter-scale tests, as its force sensor is designed with a double-beam configuration to minimize torque. If torque plays a role in nanoscale and microscale tests, the intrinsic frictional aging without influence of torque would have been even stronger. Therefore, the torque effect is also unlikely to account for the length scale effect we observed in the experiments.

According to the Bowden and Tabor friction model, adhesion-dominated friction is proportional to the true contact area of the sliding interface, A_{true}, by a scale factor τ, known as the friction shear stress [21,28,39–42]. Therefore, the friction coefficient can be expressed as $\mu = F_f/F_n = \tau \cdot (A_{\text{true}}/F_n)$. During the stationary hold period, friction increases due to interface aging, which may come from strengthening of interfacial bonds and, thereby, enhanced friction shear stress [8,24,43–45] and/or enlarged true contact area [21,22]. For silica-silica contacts, previous experimental results [24] have suggested that the

enhancement in interfacial bonds might contribute dominantly to the frictional aging. Since the contact pressures of all the tests are much less than 6 GPa, the yield stress of silica [46], we assume that the frictional aging in our experiments was primarily attributed to interfacial bond strengthening. Therefore, b can be expressed as

$$b = \frac{\Delta(\mu^{\text{peak}})}{\Delta(\ln t_h)} = \frac{\Delta(\tau^{\text{peak}})}{\Delta(\ln t_h)} \cdot \frac{A_{\text{true}}}{F_n}, \tag{1}$$

where $\Delta(\tau^{\text{peak}})$ is the increase in peak friction shear stress per increase in logarithm of hold time $\Delta(\ln t_h)$. Based on Eq. (1), the length scale dependence of b can certainly originate from the term A_{true}/F_n, because the $A_{\text{true}} \sim F_n$ relation would vary with surface morphology that is intrinsically scale dependent [40,41,47,48]. For example, for single-asperity contact, the $A_{\text{true}} \sim F_n$ relation is sensitive to the shape of the probe [29]. For rough multiasperity contact, the true contact area is typically a small fraction of the apparent contact area, which often scales linearly with the normal load with a ratio determined by the characteristics of interface roughness as illustrated in Fig. 3(b) [40,41,47,48].

To further explore whether the length scale effect of frictional aging also originates from friction shear stress, we normalized b by the steady-state friction coefficient μ^{ss} so that the contribution from the $A_{\text{true}} \sim F_n$ relation can be eliminated. The normalized parameter $\tilde{b}$ is defined as

$$\tilde{b} = \frac{b}{\mu^{\text{ss}}} = \frac{1}{\tau^{\text{ss}}} \cdot \frac{\Delta(\tau^{\text{peak}})}{\Delta(\ln t_h)}, \tag{2}$$

where τ^{ss} is the friction shear stress during steady-state sliding. As shown by the star points in Fig. 3(a), $\tilde{b}$ also changes substantially from nanometer to micrometer and to millimeter scales, which suggests that different aging rates of friction shear stress also contribute to the length scale effect of b. It should be noted that the above normalization is conducted under the assumption that the true contact area of the sliding interface is constant at peak friction and in steady-state sliding. Although the true contact area can be reduced due to viscoelasticity and/or adhesion-induced crack propagation [49], such area reduction was found to be strongly dependent on the Young's modulus of the contacting materials. For soft materials, like rubber or human skin, the area reduction behavior was prominent. However, for hard materials like metals or glass, the area reduction due to shear at the onset of slip is likely negligible [49]. Considering the high stiffness of silica in our experiments, the effect of area reduction is expected to be minimum.

To better understand the length scale effect caused by friction shear stress, a regularly patterned multiasperity RSF model was constructed by considering the elastic interaction among asperities [50]. As schematically shown

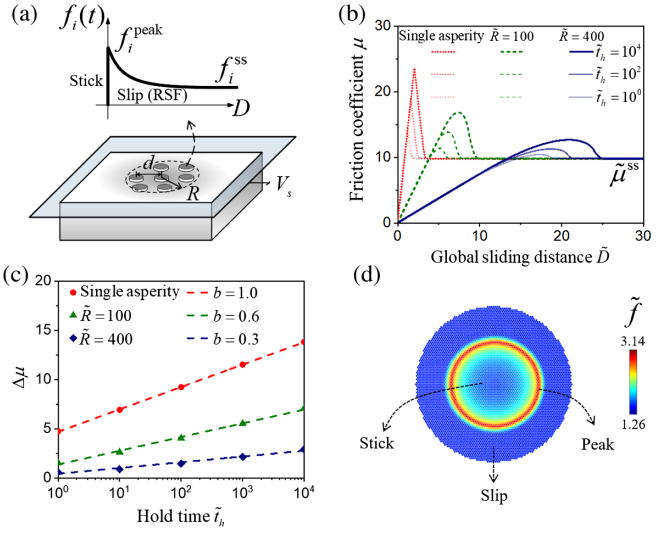

FIG. 4. (a) A schematic showing the multiasperity RSF model. (b) Frictional aging behavior of different simulation systems: single asperity, 367 asperities ($\tilde{R}=100$), and 5815 asperities ($\tilde{R}=400$). (c) Variations of friction aging coefficient with hold time for different systems. The dashed lines are log-linear fits for calculating parameter b. (d) Distribution of the normalized lateral force $\tilde{f}=f/(Er^2)$ at the moment of peak global friction for the interface with $\tilde{R}=400$. The parameters of the specific model are given in Supplemental Material, Sec. VI [26].

in Fig. 4(a), the sliding interface is formed between a rigid plane and an elastic half space with regularly patterned shallow columnar asperities with circular radius r and uniform spacing d (see more details in Supplemental Material, Sec. VI [26]). Based on the previous quasistatic model [24], the new multiasperity RSF model explicitly incorporates the RSF law to simulate the frictional aging behavior with temporal evolution. It is assumed that the frictional force of individual asperity contact follows the RSF law upon lateral displacement, i.e.,

$$f = \left[\mu_0 + a^{\text{int}} \ln\left(\frac{V}{V_0}\right) + b^{\text{int}} \ln\left(\frac{V_0\theta}{D_c^{\text{int}}}\right)\right] \cdot p, \tag{3}$$

where a^{int}, b^{int}, and D_c^{int} are the intrinsic RSF parameters for individual asperity, V is the relative velocity between the plane and the individual asperity, and p is the compressive load on each asperity. The state variable θ for individual asperity evolves according to

$$\frac{d\theta}{dt} = 1 - \frac{V\theta}{D_c^{\text{int}}}. \tag{4}$$

In the multiasperity RSF model, the interface is first held stationary for different periods of time after steady-state sliding, then the interface is reloaded, and the evolution of global friction and friction coefficient are calculated. To study the size effect, the radius of the apparent contact area

R, and thereby the number of asperities, is varied. The interasperity elastic interaction is described by the Cerruti solution from continuum mechanics [29] as described in Supplemental Material, Sec. VI [26].

Figure 4(b) shows the evolutions of the global friction coefficient in simulations of different sliding interfaces containing a single asperity and multiple asperities ($\tilde{R} = R/r = 100$ and 400) (see more details in Supplemental Material, Sec. VI [26]). For all simulation cases, the global friction coefficient would reach a peak value upon reloading and then evolve gradually to a steady-state value after a certain slide distance, consistent with the experimental observation. More importantly, the aging coefficient $\Delta\mu$ in the simulations also increases linearly with logarithm of hold time $\tilde{t}_h$, as shown in Fig. 4(c), consistent with the experimental observations. By fitting the slopes of the curves, the global parameter b can be extracted. Although the intrinsic parameter is set to be identical ($b^{\text{int}} = 1.0$) for individual asperity in all systems, the global parameters b extracted from the global behavior are 1.0, 0.6, and 0.3 for single asperity, $\tilde{R} = 100$ and $\tilde{R} = 400$, respectively. The simulation results indicate that b gets smaller and smaller as the apparent contact size increases, showing clear size dependence. Moreover, further simulation results suggest that the length scale effect revealed in the simulation is not sensitive to the specific assumptions of the asperity size and pressure distribution (see Supplemental Material, Sec. VII [26]).

Since the normal compressive load on each individual asperity is identical in our RSF model, the size dependence of b should come solely from global friction shear stress. To better understand the state of the sliding interface, we analyzed the lateral force distribution along the interface during the reloading period. As shown in Fig. 4(d), when the global friction reaches the peak value, the asperities near the contact edge have slipped, while the asperities at the center are still getting aged. This nonsynchronized slip during reloading becomes more pronounced when the apparent contact size increases (see Fig. S5(c) in Supplemental Material, Sec. VI [26], for more details), resulting in a weaker global aging effect.

In the multiasperity RSF model, the coupling between two neighboring asperities is described by the Cerruti solution, leading to a coupling compliance on the order of $\sim(G \cdot d)^{-1}$, where G is the effective shear modulus of the contacting materials (see Supplemental Material, Sec. VI [26]), while the contact compliance of an individual asperity with a shallow profile is on the order of $\sim(G \cdot r)^{-1}$. Analogous to the normal contact behavior of a regularly patterned multiasperity interface [50], the mechanical coupling of the system is determined by a nondimensional parameter $\lambda \sim d^2/(r \cdot R)$, where a larger λ value represents weaker mechanical coupling. When asperities are sparsely distributed or weakly connected, or when asperities are tall with a relatively high aspect ratio, the mechanical coupling is small and the length scale effect would be weak. In contrast, for an interface with strong interasperity coupling, the system behaves much like a smooth contact, and the length scale effect would become stronger. In this case, the level of frictional aging decays as R increases. However, this decay will not go infinitely; instead, it will converge to a steady value due to multidislocation mediated slip when the contact reaches a critical size [51]. This critical size should be determined by the "effective Peierls stress" of the rough rock interface, whose value will depend on the mechanical properties of the rocks and interface roughness. A more systematic study on this particular aspect may help explain why parameter b in macroscopic friction experiments of rock materials mostly lies between 0.001 and 0.015 [19,21,25], instead of approaching 0 as predicted by our idealized model.

In conclusion, frictional aging experiments with apparent contact size spanning across 3 orders of magnitude have provided direct experimental evidence that there exists a strong length scale effect in frictional aging of silica-silica contacts. Theoretical analysis suggests that such a pronounced length scale effect originates both from the roughness-dependent true contact area-load relation and scale-dependent friction shear stress. The latter mechanism can be explained by considering the nonsynchronized slip behavior in a multiasperity RSF model. The scaling effect of frictional aging deepens our understandings of the universality of the widely used RSF laws and enables more physically meaningful predictions from these empirical models.

This work was funded by the National Natural Science Foundation of China (Grants No. 11772169, No. 11921002, and No. 11890671), the Initiative Program of State Key Laboratory of Tribology (SKLT2019B02), and the National Science and Technology Major Project (2017-VI-0003-0073). S. L. thanks Dr. Lin Ge from NT-MDT Beijing Office for helping develop a code for AFM slide-hold-slide tests, Dr. Shuwei Liu and Professor Tianbao Ma both from Department of Mechanical Engineering, Tsinghua University for helping prepare silica microsphere probes, and Dr. Muqiang Jian and Professor Yingying Zhang both from Department of Chemistry, Tsinghua University for helping oxidize Si substrates. The authors are grateful to the anonymous reviewers who helped improve the quality of the manuscript notably.

*Present address: Department of Mechanical Engineering, Imperial College London, London SW7 2AZ, United Kingdom.

†To whom correspondence should be addressed. qunyang@tsinghua.edu.cn

[1] J. H. Dieterich, J. Geophys. Res. **84**, 2161 (1979).
[2] A. Ruina, J. Geophys. Res. **88**, 10359 (1983).
[3] K. A. Grosch, Proc. R. Soc. A **274**, 21 (1962).
[4] T. Baumberger and C. Caroli, Adv. Phys. **55**, 279 (2006).

[5] B. Lishman, P. R. Sammonds, and D. L. Feltham, Cold Reg. Sci. Technol. **90–91**, 9 (2013).
[6] F. Heslot, T. Baumberger, B. Perrin, B. Caroli, and C. Caroli, Phys. Rev. E **49**, 4973 (1994).
[7] A. D. Corwin and M. P. de Boer, J. Microelectromech. Syst. **18**, 250 (2009).
[8] Y. Liu and I. Szlufarska, Phys. Rev. Lett. **109**, 186102 (2012).
[9] M. Feldmann, D. Dietzel, A. Tekiel, J. Topple, P. Grutter, and A. Schirmeisen, Phys. Rev. Lett. **117**, 025502 (2016).
[10] S. Dillavou and S. M. Rubinstein, Phys. Rev. Lett. **120**, 224101 (2018).
[11] M. Vorholzer, J. G. Vilhena, R. Perez, E. Gnecco, D. Dietzel, and A. Schirmeisen, Phys. Rev. X **9**, 041045 (2019).
[12] K. Tian, Z. Li, Y. Liu, N. N. Gosvami, D. L. Goldsby, I. Szlufarska, and R. W. Carpick, Phys. Rev. Lett. **124**, 026801 (2020).
[13] S. S. Shroff, N. Ansari, W. R. Ashurst, and M. P. de Boer, J. Appl. Phys. **116**, 244902 (2014).
[14] S. S. Shroff and M. P. de Boer, Tribol. Lett. **63**, 39 (2016).
[15] S. S. Shroff and M. P. de Boer, Tribol. Lett. **63**, 31 (2016).
[16] J. R. Rice, N. Lapusta, and K. Ranjith, J. Mech. Phys. Solids **49**, 1865 (2001).
[17] S. T. Tse and J. R. Rice, J. Geophys. Res. **91**, 9452 (1986).
[18] T. E. Tullis, Pure Appl. Geophys. **126**, 555 (1988).
[19] C. Marone, Annu. Rev. Earth Planet Sci. **26**, 643 (1998).
[20] J. R. Rice and A. L. Ruina, J. Appl. Mech. **50**, 343 (1983).
[21] J. H. Dieterich and B. D. Kilgore, Pure Appl. Geophys. **143**, 283 (1994).
[22] J. H. Dieterich and G. Conrad, J. Geophys. Res. **89**, 4196 (1984).
[23] D. L. Goldsby and T. E. Tullis, Geophys. Res. Lett. **29**, 25-1 (2002).
[24] Q. Li, T. E. Tullis, D. Goldsby, and R. W. Carpick, Nature (London) **480**, 233 (2011).
[25] R. M. Skarbek and H. M. Savage, Geosphere **15**, 1665 (2019).
[26] See Supplemental Material at http://link.aps.org/supplemental/10.1103/PhysRevLett.125.215502 for details of sample preparation, characteristic distance fitting, contact size and contact pressure estimation, friction vs load curves for experiments at three length scales, effect of relative humidities, multiasperity RSF model, and simulation results of uniform and Hertzian contact pressure, which includes Refs. [8,27–32].
[27] B. V. Derjaguin, V. M. Muller, and Y. P. Toporov, Prog. Surf. Sci. **45**, 131 (1994).
[28] J. F. Archard, Proc. R. Soc. A **243**, 190 (1957).
[29] K. L. Johnson, *Contact Mechanics* (Cambridge University Press, Cambridge, England, 1987).
[30] D. B. Asay, M. P. de Boer, and S. H. Kim, J. Adhes. Sci. Technol. **24**, 2363 (2010).
[31] F. Musso, P. Mignon, P. Ugliengo, and M. Sodupe, Phys. Chem. Chem. Phys. **14**, 10507 (2012).
[32] L. M. Qian, F. Tian, and X. D. Xiao, Tribol. Lett. **15**, 169 (2003).
[33] Q. Li and K.-S. Kim, Proc. R. Soc. A **464**, 1319 (2008).
[34] J. N. Israelachvili, *Intermolecular and Surface Forces* (Academic Press, London, 1992).
[35] A. Kumar, T. Staedler, and X. Jiang, Beilstein J. Nanotechnol. **4**, 66 (2013).
[36] N. M. Beeler, T. E. Tullis, and J. D. Weeks, Geophys. Res. Lett. **21**, 1987 (1994).
[37] Z. Li, L. Pastewka, and I. Szlufarska, Phys. Rev. E **98**, 023001 (2018).
[38] S. Dillavou and S. M. Rubinstein, Phys. Rev. Lett. **124**, 085502 (2020).
[39] F. P. Bowden and D. Tabor, *The Friction and Fubrication of Solids* (Oxford University Press, New York, 1958).
[40] J. A. Greenwood and J. B. P. Williamson, Proc. R. Soc. A **295**, 300 (1966).
[41] B. N. Persson, O. Albohr, U. Tartaglino, A. I. Volokitin, and E. Tosatti, J. Phys. Condens. Matter **17**, R1 (2005).
[42] Y. F. Mo, K. T. Turner, and I. Szlufarska, Nature (London) **457**, 1116 (2009).
[43] K. Tian, D. L. Goldsby, and R. W. Carpick, Phys. Rev. Lett. **120**, 186101 (2018).
[44] A. Li, Y. Liu, and I. Szlufarska, Tribol. Lett. **56**, 481 (2014).
[45] K. Tian, Z. Li, N. N. Gosvami, D. L. Goldsby, I. Szlufarska, and R. W. Carpick, ACS Nano **13**, 7425 (2019).
[46] D. Torres-Torres, J. Muñoz-Saldaña, L. A. Gutierrez-Ladron-de Guevara, A. Hurtado-Macías, and M. V. Swain, Model. Simul. Mater. Sci. Eng. **18** (2010).
[47] M. H. Muser, Phys. Rev. Lett. **100**, 055504 (2008).
[48] M. Ciavarella, V. Delfine, and G. Demelio, J. Mech. Phys. Solids **54**, 2569 (2006).
[49] R. Sahli, G. Pallares, C. Ducottet, I. E. B. Ali, S. Al Akhrass, M. Guibert, and J. Scheibert, Proc. Natl. Acad. Sci. U.S.A. **115**, 471 (2018).
[50] S. Li, Q. Yao, Q. Li, X.-Q. Feng, and H. Gao, J. Mech. Phys. Solids **111**, 277 (2018).
[51] J. A. Hurtado and K. S. Kim, Proc. R. Soc. A **455**, 3385 (1999).